6-7-2006

Cold Event in the South Atlantic Bight During Summer of 2003: Anomalous Hydrographic and Atmospheric Conditions

Alfredo Aretxabaleta
University of North Carolina

James R. Nelson
Skidaway Institute of Oceanography

Jack O. Blanton
Skidaway Institute of Oceanography

Harvey E. Seim
University of North Carolina

Francisco E. Werner
University of North Carolina

See next page for additional authors

Tide, buoyancy, and wind-driven circulation of the Charlotte Harbor estuary: A model study

Lianyuan Zheng and Robert H. Weisberg
College of Marine Science, University of South Florida, St. Petersburg, Florida, USA

Received 6 June 2003; revised 7 April 2004; accepted 16 April 2004; published 10 June 2004.

[1] The circulation of the Charlotte Harbor (CH) estuary is explored with a primitive equation model that encompasses the estuary and the adjacent West Florida Shelf. Tidal forcing is from the shelf through the inlets. We use the M_2, S_2, K_1, and O_1 constituents that account for 95% of the shelf tidal variance. River inflows are by the Peace, Myakka, and Caloosahatchee Rivers at their spring 1998 mean values. Wind effects are considered for upwelling or downwelling favorable winds that are either held constant or allowed to oscillate with varying periodicities. These factors are sequentially added to look at their individual and collective influences on the estuary's circulation and salinity fields. Tidal currents are asymmetric and slightly ebb dominant during spring tides. River inflows, combined with tidal mixing, result in a net estuarine circulation by gravitational convection, and the Coriolis acceleration causes the outflowing currents to be stronger and with lower salinity on the western side of the CH portion of the estuary. By virtue of shallow connecting passages the CH portion acts nearly independently from the San Carlos Bay portion of the combined CH estuary system. The addition of wind affects both the instantaneous and net circulation and salinity distributions by increasing mixing and by imposing a force that may add either constructively or destructively to the gravitational convection. The net up-estuary salt flux is also affected by tides and winds through their contributions to the Reynolds' flux, which exceeds the salt flux by gravitational convection alone. *INDEX TERMS:* 4235 Oceanography: General: Estuarine processes; 4251 Oceanography: General: Marine pollution; 4815 Oceanography: Biological and Chemical: Ecosystems, structure and dynamics; *KEYWORDS:* model study, estuarine circulation

Citation: Zheng, L., and R. H. Weisberg (2004), Tide, buoyancy, and wind-driven circulation of the Charlotte Harbor estuary: A model study, *J. Geophys. Res.*, *109*, C06011, doi:10.1029/2003JC001996.

1. Introduction

[2] The Charlotte Harbor (CH) estuary (Figure 1) is the second largest estuarine system in Florida. It is shallow (with a mean depth of 2 m) and geometrically complex, consisting of two primary regions, the CH and San Carlos Bay (SCB), connected by Pine Island Sound and Matlacha Pass. The estuary spans some 800 km^2, and it connects with the adjacent Gulf of Mexico, West Florida Shelf (WFS) through three primary inlets: Boca Grande Pass (BGP), Captiva Pass, and the mouth of SCB, and through lesser inlets across the system of barrier islands that separate the estuary from the WFS. These barrier islands include the tourist destinations of the Sanibel and Captiva Islands.

[3] The circulation of the CH estuary results from the combined effects of tides, rivers, and winds. Tides are imposed by the WFS, where the M_2, S_2, K_1, and O_1 constituents account for about 95% of the tidal variance [*He and Weisberg*, 2002]. With form ratio $[(K_1 + O_1)/(M_2 + S_2)]$ of 1 to 1.5, the CH estuary's tidal regime is of mixed, mainly semidiurnal type [*Goodwin and Michaelis*, 1976]. Constructive and destructive inference between these diurnal and semidiurnal constituents results in a diurnal inequality and a fortnightly spring and neap tide cycle. Along with larger (smaller) amplitudes during spring (neap) tide, the spring (neap) tides are more diurnal (semidiurnal) in character.

[4] Fresh water enters through by the Peace, Myakka, and Caloosahatchee Rivers. The discharge rates of the Peace and Myakka Rivers that feed the CH side of the estuary are directly related to drainage basin rainfall, with maximum and minimum values occurring in August–September and April–May, respectively. The discharge rate of the Caloosahatchee River that feeds the SCB side of the estuary is controlled by regulatory releases from Lake Okeechobee [*Doering and Chamberlain*, 1999]. The Peace and Caloosahatchee Rivers have comparable volume flow rates, while the Myakka River is an order of magnitude smaller. Maximum discharge rates may exceed 350 m^3/s for the Peace River and 450 m^3/s for the Caloosahatchee River during wet years.

[5] Winds over the CH estuary vary seasonally. Climatology [e.g., *Hellerman and Rosenstein*, 1983] shows prevailing offshore winds (northeasterly to easterly) from September to February, followed by a spring transitional

0148-0227/04/2003JC001996

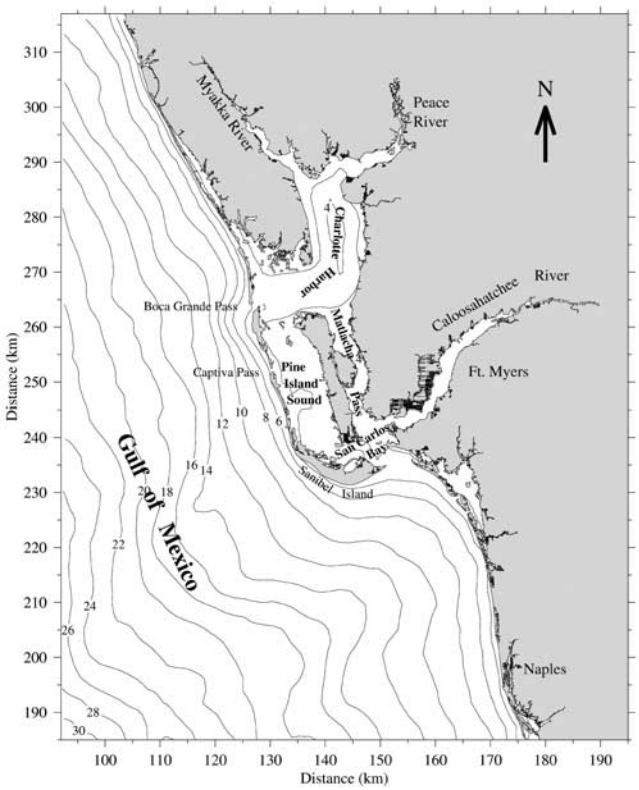

Figure 1. The geometry and bathymetry of the Charlotte Harbor estuary and the adjacent West Florida Shelf.

regime (March to May) in which the winds shift from easterly to southeasterly. Weak southeasterly winds then prevail from June to August. The climatology is punctuated by synoptic-scale variability as extratropical weather systems propagate across the region in fall through spring. During spring and summer the winds are also impacted by sea breeze and tropical storms. Generally, with the exception of tropical storms the winds tend to be strongest in response to the extratropical weather patterns from fall through spring.

[6] Material properties respond to the variations in rivers, tides, and winds. Seasonal salinity variations occur primarily in response to seasonal river discharge variations, whereas daily salinity variations occur primarily in response to tides, with highest (lowest) salinity values occurring at slack high (low) water. Observations (E. Estevez, Mote Marine Laboratory, personal communication) show that the CH estuary may be classified as partially to well-mixed except during high river discharge periods when the water column may be highly stratified.

[7] A model study by *Goodwin* [1996] demonstrated agreements for tidal currents and sea level when gauged against data. That model, being two-dimensional (vertically averaged) and exclusive of winds, was neither capable of describing the salinity structure, nor the effects of wind on the stratification or flow fields. Thus the physical mechanisms that drive the nontidal, density-driven estuarine circulation and the wind-driven variations of the circulation remain to be described for the CH estuary. Since these aspects of the circulation largely control both the stratification and the related state variable distributions, a more complete understanding of the circulation is necessary to support multidisciplinary ecological studies.

[8] Here we use a three-dimensional, primitive equation model to investigate the tide, buoyancy, and wind-driven circulations of the CH estuary and the exchanges of water that occur between the estuary and the adjacent WFS. Section 2 describes the model and the experimental design. Section 3 presents the tidal portion of the model simulations. River discharges are added in section 4 to examine the buoyancy effects on the circulation and salinity fields. Constant winds in either downwelling or upwelling favorable directions are then added in section 5 to examine the roles of all three forcing elements on the circulation and salinity fields. Since winds tend to be oscillatory in nature, we examine this effect in section 6, and the results are summarized in section 7.

2. Model Description

[9] We use the primitive equation, ECOM3D-si model, based on the Princeton Ocean Model (POM) of *Blumberg and Mellor* [1987] as subsequently modified by *Blumberg* [1993], *Chen and Beardsley* [1995], and *Zheng et al.* [2003]. The model incorporates the *Mellor and Yamada* [1982] level 2.5 turbulence closure scheme to provide flow-dependent turbulent mixing parameters along with a free surface. A σ coordinate in the vertical and an orthogonal curvilinear coordinate in the horizontal are used. Unlike POM that employs a mode-splitting technique, ECOM3D-si uses a semi-implicit finite difference scheme in which the advection, Coriolis, baroclinic pressure gradient, and horizontal diffusion terms are calculated explicitly, and the barotropic pressure gradient (or surface elevation gradient) and the vertical diffusion terms are solved for implicitly. Advantages of this semi-implicit scheme are: (1) it generates a symmetric, positive definite set of equations for sea level that can be solved by a preconditioned conjugate gradient method [*Casulli*, 1990] and (2) it removes the external CFL constraint allowing for larger time steps by eliminating the need for separate internal and external modes. Successful applications of ECOM3D-si exist for ocean [e.g., *Mellor and Ezer*, 1991], coastal [e.g., *Blumberg et al.*, 1993; *Chen and Beardsley*, 1995; *Chen et al.*, 1999], and estuarine [e.g., *Blumberg and Pritchard*, 1997; *Zheng et al.*, 2003] environments.

[10] A common problem to the salinity equation, when central differences are used for the advection terms, is the occurrence of negative salinity if the estuary is shallow and the river discharge is large. To avoid this we employ the Multidimensional Positive Definite Advection Transport Algorithm [*Smolarkiewicz*, 1984] that uses an ''antidiffusion'' velocity in a successive upwind scheme to correct first-order truncation errors, yielding a positive definite, second-order accurate advection scheme. Successful applications of this scheme exist for nutrient transport studies on Georges Bank [*Chen and Beardsley*, 1998] and for salinity simulations in the Satilla River estuary [*Zheng et al.*, 2003].

[11] The model grid is shown in Figure 2, with an open boundary located on the shelf some 30 km away from the barrier islands. A shelf component is necessary for two reasons. First, with multiple inlets, the only way to specify the estuary's tidal forcing is to apply a shelf tide model.

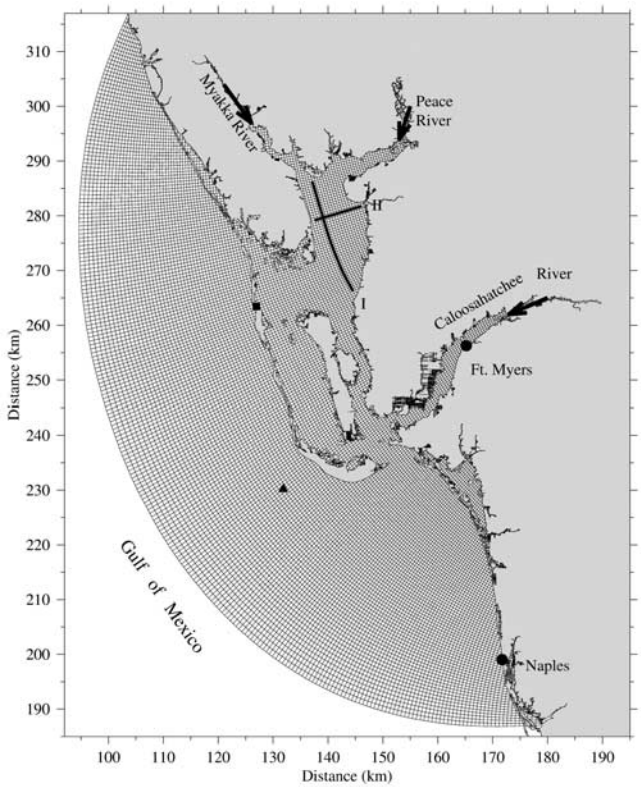

Figure 2. The model grid showing the along-axis (I) and across-axis (II) sections (bold lines) chosen for analyses and the tide gauge (solid circles) and current meter (solid triangle) stations for model simulation comparisons. The square denotes a site located just inside of Boca Grande Pass at which we present tidal current profiles.

Second, the shelf component allows us to address the material exchanges between the shelf and the estuary. The model grid extends out to the 25 m isobath, arching to the coast near Venice, Florida in the north and Naples, Florida. in the south. There are 250 (along-shelf) $\times$ 148 (across-shelf) grid points varying in resolution from about 250 m inside the estuary to about 1100 m at the open boundary. Eleven evenly distributed σ levels provide vertical resolution of less than 0.1 m in shallow regions to between 1 $\sim$ 2 m on the innershelf. We use National Ocean Service bathymetry data with 30 m resolution over most of the domain. In regions such as the Caloosahatchee River and Matlacha Pass, where bathymetry data are not given in this database, we digitized bathymetry directly from NOAA charts. A time step of 124.2 s (equating to 360 time steps per M_2 tide cycle) is used.

[12] Model runs begin from a state of rest with initial salinity and temperature values set at 35 psu and 20°C, respectively. At the open boundary sea level is controlled using the M_2, S_2, K_1, and O_1 constituents sampled from the *He and Weisberg* [2002] WFS tide model, and a radiation boundary condition with a propagation speed of $\sqrt{gh}$ is used for velocity. Temperature is held constant throughout, and a nongradient open boundary condition is applied to salinity such that outgoing water may leave with its prognostic salinity, whereas incoming water enters with a salinity of 35 psu. To avoid instability the tidal amplitudes are ramped up from zero to their full values over the first M_2 tide cycle.

[13] Three different classes of experiments are conducted. The first is a barotropic tide simulation. The second includes tides and rivers with prognostic salinity. The third adds either constant or oscillatory winds to the tide, plus river case.

3. Tides

[14] After the initial ramp up over one M_2 tide cycle the model is run to quasi-equilibrium over an additional 9 M_2 cycles. Sixty more M_2 cycles are then run for analysis. We employ a linear least squares harmonic analysis (following *Foreman* [1977, 1978]) to compute the amplitudes, phases, and current ellipse parameters for the M_2, S_2, K_1, and O_1 constituents at each of the model grid points. The model-predicted tidal elevations agree well with observations at the Naples and Ft. Myers tide gauges (Figure 3). The model duplicates the spring to neap tide variation, including the more diurnal (semidiurnal) character at spring (neap) tide. The simulation at Naples is better than at Ft. Myers since Naples is closer to the open boundary where the tides are forced and Ft. Myers is affected by depth and geometry complexities. We found that by improving the bathymetric data from the Caloosahatchee River we improved the Ft. Myers simulation. Along with these sea level comparisons, Table 1 shows the observed and computed tidal current ellipse parameters at a mooring positioned southwest of

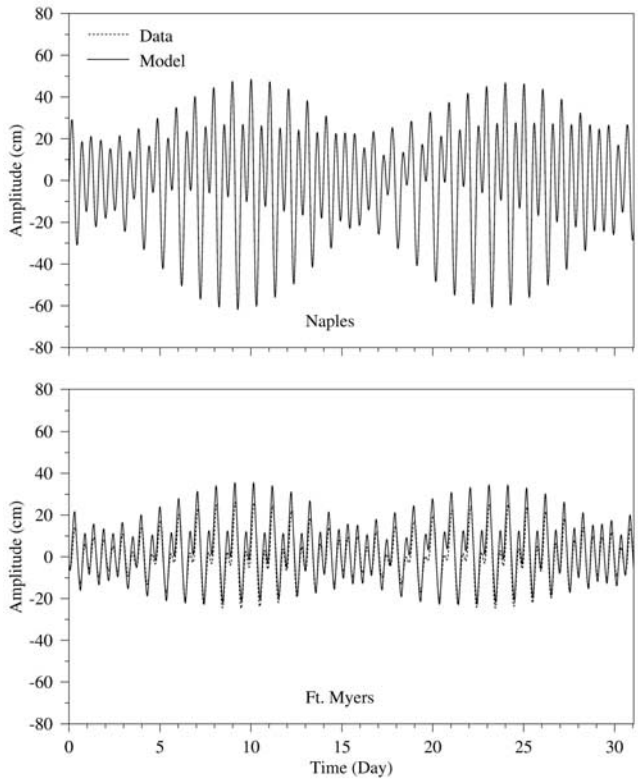

Figure 3. Comparisons between modeled (solid lines) and observed (dashed lines) tidal elevations at Naples and Ft. Myers based on summations of the principal M_2, S_2, K_1, and O_1 constituents.

Table 1. A Comparison of M_2, S_2, K_1, and O_1 Tidal Ellipse Parameters Observed and Modeled at a Current Meter Station Moored Offshore of Sanibel Island[a]

	Observed			Modeled		
	U_{major}, m s^{-1}	U_{minor}, m s^{-1}	α, deg	U_{major}, m s^{-1}	U_{minor}, m s^{-1}	α, deg
M_2	0.143	−0.020	151	0.123	−0.005	141
S_2	0.059	−0.010	151	0.045	−0.004	141
K_1	0.034	−0.007	135	0.029	−0.014	143
O_1	0.035	−0.014	134	0.033	−0.013	143

[a]See also Figure 2. The ellipse orientation α is measured counterclockwise from the east and the negative sign of U_{minor} indicates a clockwise polarization.

Sanibel (see Figure 2). Combined, the sea level and velocity comparisons demonstrate the legitimacy of the open boundary condition in forcing the tides.

[15] Model-predicted coamplitude and cophase charts for the M_2, S_2, K_1, and O_1 tidal constituents are presented in Figures 4a and 4b, respectively. The local innershelf results are consistent with the shelf-wide findings of *He and Weisberg* [2002]. The semidiurnal species show amplitude gradients from north to south, whereas the diurnal species are spatially more uniform. The tides propagate across the innershelf and into the estuary through BGP, Captiva Pass, and the mouth of SCB. Through BGP, the M_2, S_2, K_1, and O_1 constituent amplitudes first decrease by 2.5 cm, 2 cm, 1 cm, and 1 cm, respectively, before increasing farther north into the Peace River by 6 cm, 3 cm, 1.5 cm, and 2 cm,

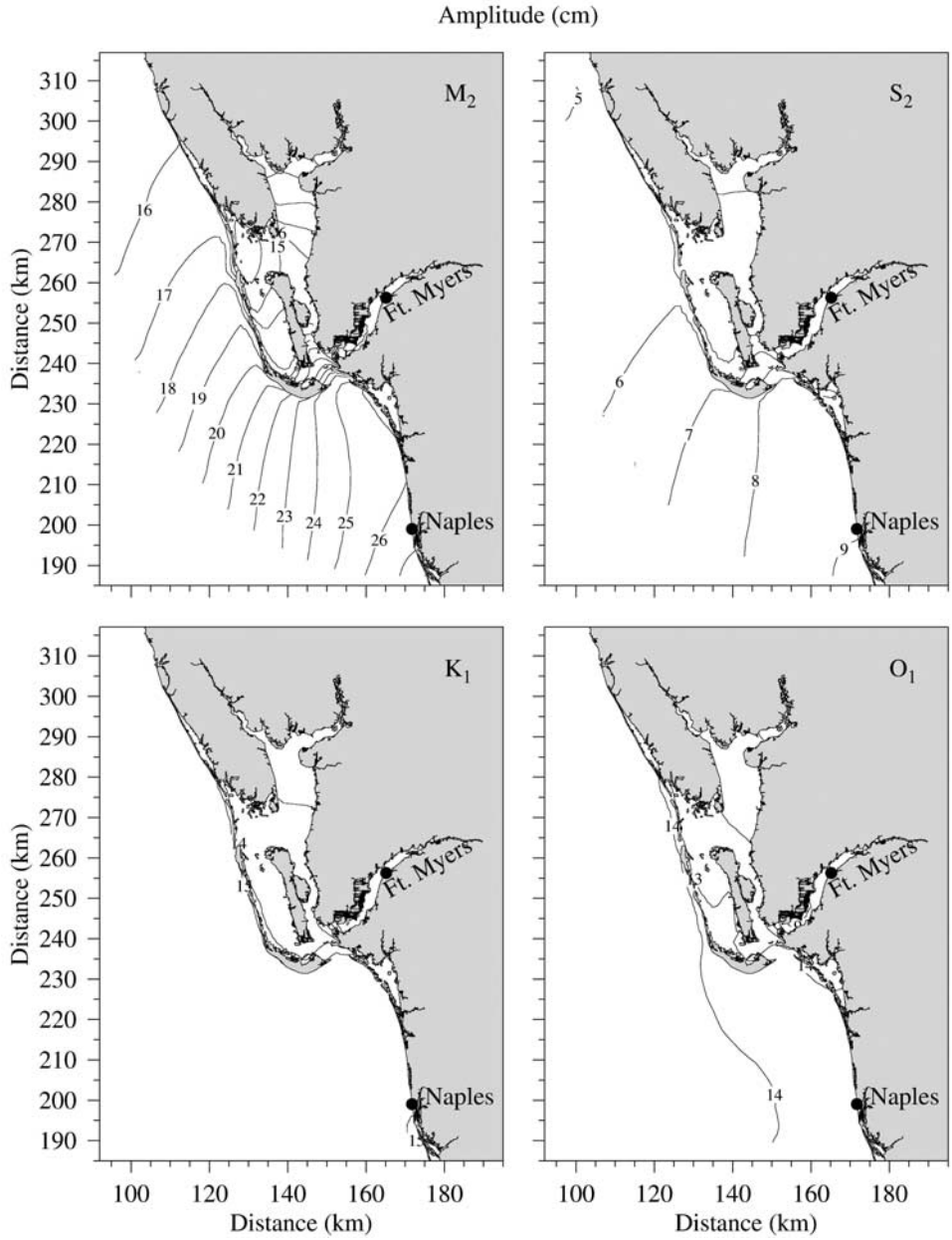

Figure 4a. Modeled coamplitude maps for the M_2, S_2, K_1, and O_1 tidal constituents. The contour interval is 1 cm.

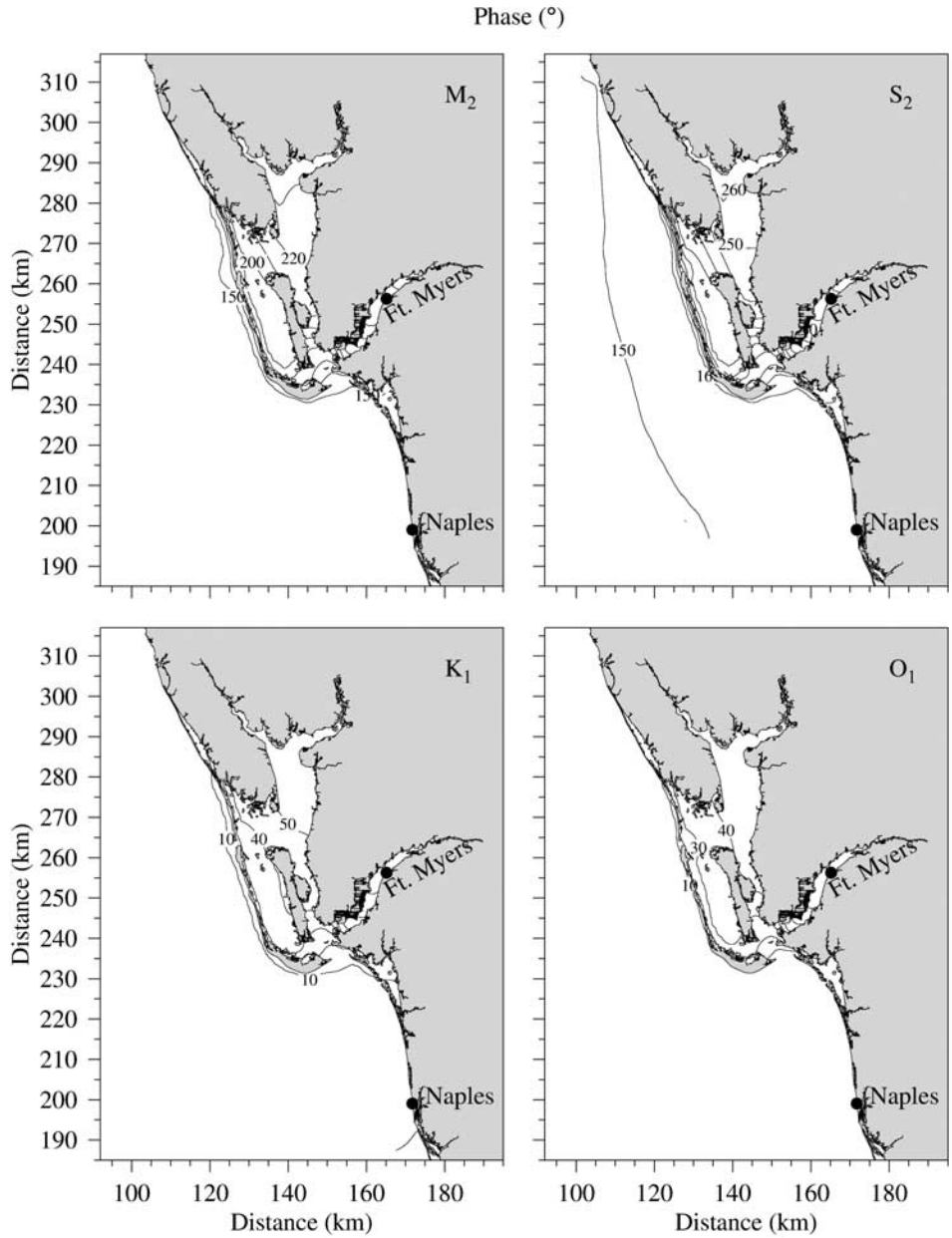

Figure 4b. Modeled cophase maps for the M_2, S_2, K_1, and O_1 tidal constituents. Phase is relative to the Greenwich meridian, and the contour interval is 10°.

respectively. The initial decrease across the inlet is by dissipation. The subsequent increase is by wave reflection at the estuary's head. Because of the narrowness of the inlet and dissipation a sufficient pressure head (by Bernoulli's theorem) is required to drive water through the inlet. This is achieved by the phase gradient across the inlet. Thus the M_2, S_2, K_1, and O_1 constituents' phases increase across the inlet by about 35°, 45°, 20°, and 20°, respectively. They continue increasing toward the Peace River by amounts larger than implied for a gravity wave propagating at speed $\sqrt{gh}$, which is consistent with frictional loses within the estuary [*Friedrichs and Madsen*, 1992]. The amplitude and phase behaviors into the estuary from the SCB entrance are somewhat different. The amplitudes decrease monotonically because of the shoaling depths into Matlacha Pass and Pine Island Sound (a frictional effect). They also decrease into the Caloosahatchee River toward Ft. Myers because of both friction and the several right angle bends in the channel, each requiring a drop in pressure. For example, the amplitude of the M_2 tide drops some 12 cm between the SCB entrance and Ft. Myers, and the phase advances substantially.

[16] The model-predicted surface currents at the maximum flood and ebb phases of a spring tide are shown in Figure 5. At maximum flood, the currents over the innershelf are weak. As water converges on the inlets the currents accelerate and are much stronger. They are a maximum at the BGP, attaining speeds of about 1.4 m s^{-1}. Currents through the SCB entrance are smaller since that inlet is wider. These currents flow into Matlacha Pass, Pine Island Sound, and the Caloosahatchee River. At maximum ebb, the currents are

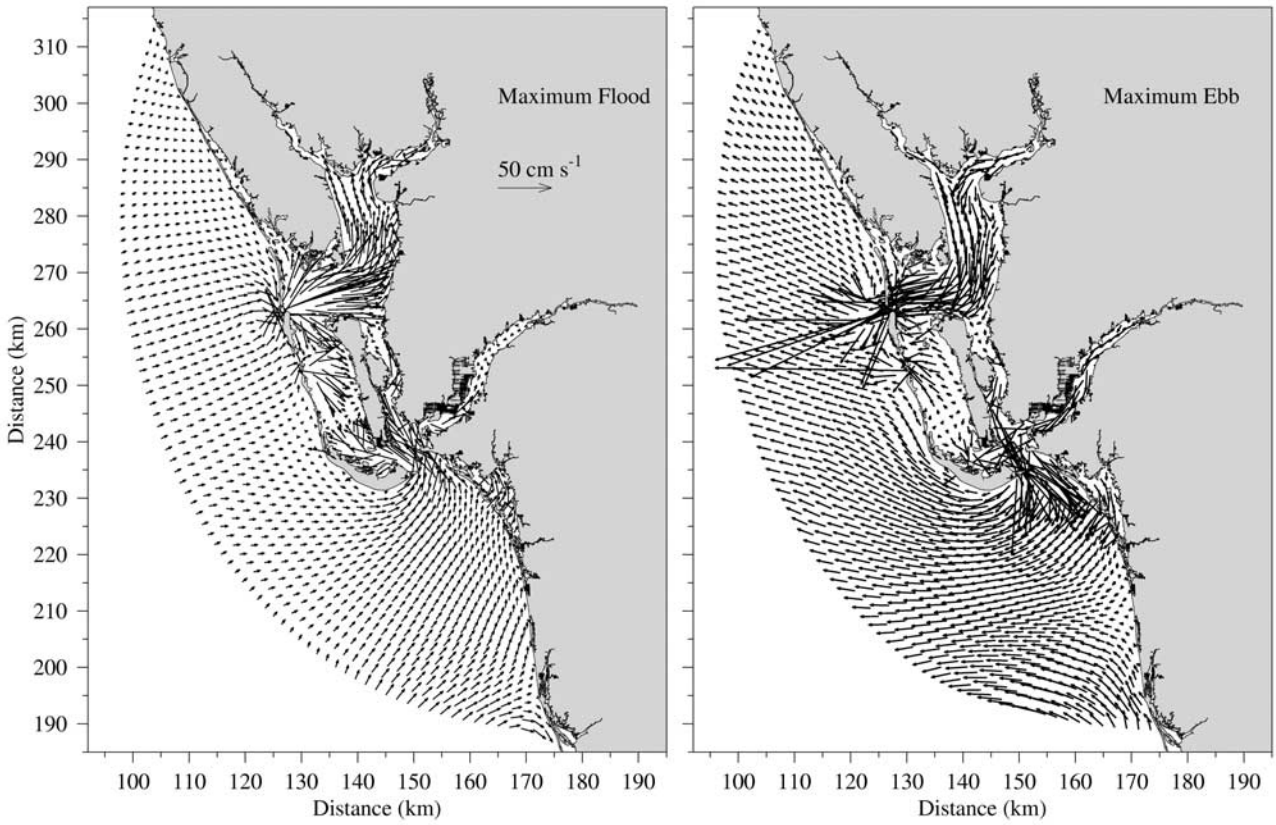

Figure 5. Tidal current vector maps sampled at the surface for the maximum (left) flood and (right) ebb tidal phases during spring tides. Modeled vectors are plotted at every third grid point.

reversed and stronger (except in the regions of Pine Island Sound and Matlacha Pass). At BGP, for example, the maximum ebb current is 1.5 m s^{-1}. Consistent with the observations of *Goodwin* [1996], these findings suggest that the CH estuary is slightly ebb dominant. Further evidence of ebb dominance (not shown) derives from the durations of the ebb and flood tides. Sampled along sections from BGP to the Peace River the flood phase is found to exceed the ebb phase of the tide by approximately 2.0 to 0.5 hours. The ebb-flood asymmetry is much less during neap tides (Figure 6), and this finding is consistent with other estuaries as reported by *Aubrey and Speer* [1985]. With asymmetry deriving from nonlinear interaction it follows that asymmetry should decrease with decreasing amplitude from spring to neap tide.

[17] Strong tidal currents induce vertical velocity variations at the passes. Figure 6 shows spring and neap tide vertical velocity distributions at BGP for the slack high, slack low, and the maximum ebb and flood phases. Maximum ebb (flood) shows downwelling (upwelling) at the location sampled just inside the pass with an ebb-flood asymmetry and with the spring tide values about twice those at neap tide. These behaviors may be explained by the topographic variations along the channel axis (with maximum depth within the inlet) and the bottom kinematic boundary condition.

4. Tides, Plus Rivers

[18] Following the procedure of section 3 river discharges are switched on [as a volume flux boundary condition [*Chen et al.*, 1999] after 10 M_2 cycles and then held constant for 120 M_2 cycles to allow the model-predicted salinities to reach a quasi-steady state. We use the spring 1998 mean discharges of 165, 40, and 240 m^3 s^{-1} for the Peace, Myakka, and Caloosahatchee Rivers, respectively. Since spring 1998 was anomalously wet these values are meant to reflect conditions of large river inflows. In this section we show results that are averaged over the next two M_2 cycles to explore the nontidal circulation and salinity fields determined by the combined effects of tides and rivers.

[19] The nontidal currents are strongly affected by rivers since (with tidal mixing) these impart the gravitational convection portion of the circulation that is generally referred to as estuarine circulation [e.g., *Cameron and Pritchard*, 1963]. Figure 7 shows the tide-averaged surface current and salinity fields. Waters from the Peace and Myakka Rivers converge, and the combined flow then proceeds southward down the main body of the estuary. Note that the tide-averaged currents are stronger on the western side, as is also reflected by the lower-salinity values there. A model twin experiment (not shown) omitting the Coriolis acceleration gave different results, with the current and salinity fields being more symmetric about the estuary axis and driven by a concave sea surface height due to the centrifugal acceleration. This twin experiment demonstrates that the right hand side preference when looking downstream is a consequence of the Coriolis acceleration.

[20] From both the velocity and salinity patterns we see that the estuary partitions into two units, a CH side, influenced by the Peace and Myakka Rivers, and a SCB

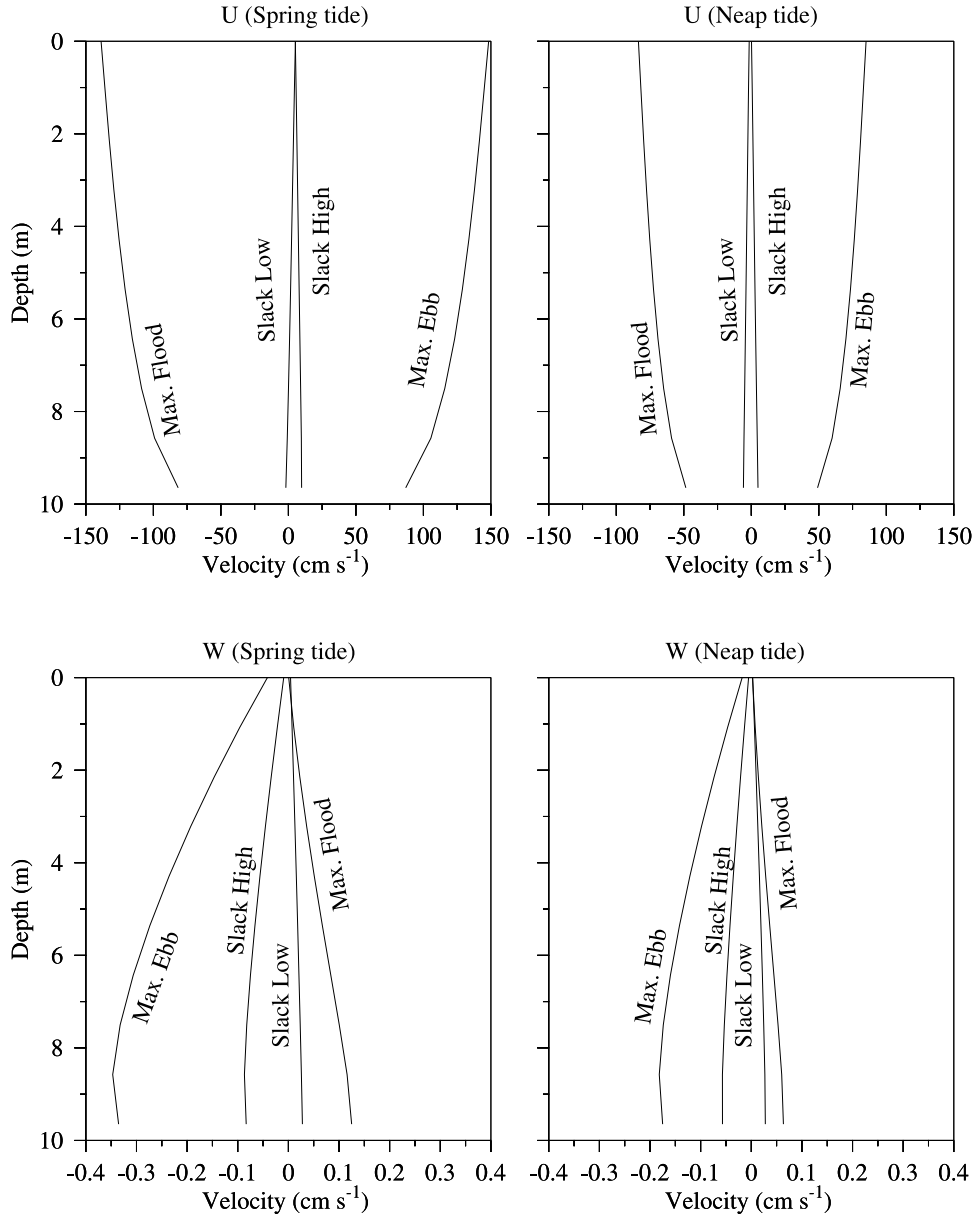

Figure 6. Vertical profiles of the (top) horizontal and (bottom) vertical components of velocity sampled at Boca Grande Pass for tidal phases corresponding to slack high water, slack low water, maximum flood, and maximum ebb during (left) spring tides and (right) neap tides.

side, influenced by the Caloosahatchee River. Separating these two units are the shallow Matlacha Pass and Pine Island Sound regions. Effectively, the system consists of two nearly independent estuaries. Fresh water from Caloosahatchee River exits primarily through the mouth of SCB, whereas fresh water from the Peace and Myakka Rivers exits primarily through BGP.

[21] Once on the innershelf waters emanating from the CH estuary are affected by the local topography and the Coriolis acceleration with the outflows sweeping in broad anticyclonic arcs. The salinity field reflects this behavior, with a near surface lens of relatively low-salinity water organizing into a northward-directed current.

[22] Returning to the estuary, a sampling of the tide-averaged circulation and salinity in a vertical plane oriented along the main channel axis (the bold line I in Figure 2) reveals a two-layered net estuarine circulation (Figure 8) with fresher water flowing seaward atop saltier water flowing landward, as expected by gravitational convection. The maximum down-estuary current (within the upper 1 m of the water column) is about 0.12 m s^{-1}, compared with the maximum up-estuary current of 0.06 m s^{-1}. On cross-sectional average, the net transport equals the river discharge rate. Note that before diminishing and reversing sign along this section the outflowing water turns right to exist through BGP.

[23] The vertical structures of the estuarine circulation and the salinity stratification are largely determined by tidal mixing. Since tidal mixing originates from friction along the bottom the salinity isolines of Figure 8 are nearly vertical

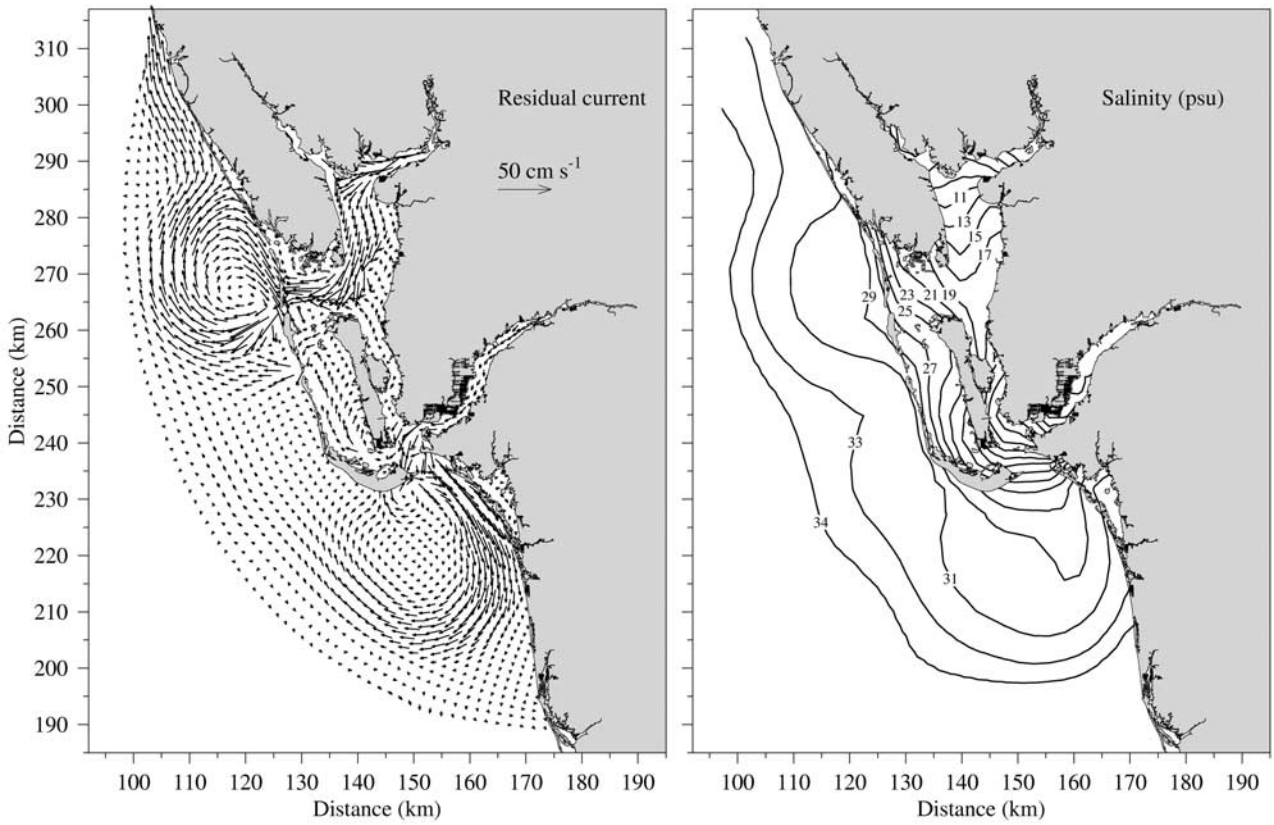

Figure 7. Surface (left) current vector and (right) salinity maps for the case of tides, plus rivers, averaged over two M_2 cycles. The contour interval for salinity is 1 psu, and the vectors are plotted at every third grid point.

there, as contrasted with the isolines being more nearly horizontal at the surface.

5. Tides, Plus Rivers, Plus Downwelling or Upwelling Favorable Winds

[24] Estuaries are also influenced by winds, either directly by the stress on the estuary surface [*Weisberg and Sturges*, 1976; *Weisberg*, 1976], or indirectly by wind stress effects on the adjacent coastal ocean [*Wang*, 1979]. We begin to address this for the CH estuary by forcing the model with spatially uniform winds directed either toward the northwest or the southeast. Typical of winds for the region we use a speed of 5 m s^{-1}. Adding to section 4 the model is spun up to tides over 10 M_2 cycles, then to rivers over 120 M_2 cycles, and then to the uniform winds over another 10 M_2 cycles.

[25] The wind directions are intended to explore three factors. First, with respect to the WFS, southeasterly (northwesterly) winds are downwelling (upwelling) favorable. They cause onshore (offshore) Ekman transports and along-shore currents directed toward the northwest (southeast) [e.g., *Li and Weisberg*, 1999]. Second, with respect to the estuary, they act in opposition to (or in concert with) the two-layered estuarine circulation induced by gravitational convection (Figure 8). Third, by adding an additional source for mixing from the surface down to go along with the tidal mixing from the bottom up the winds largely alter the estuary's salinity structure.

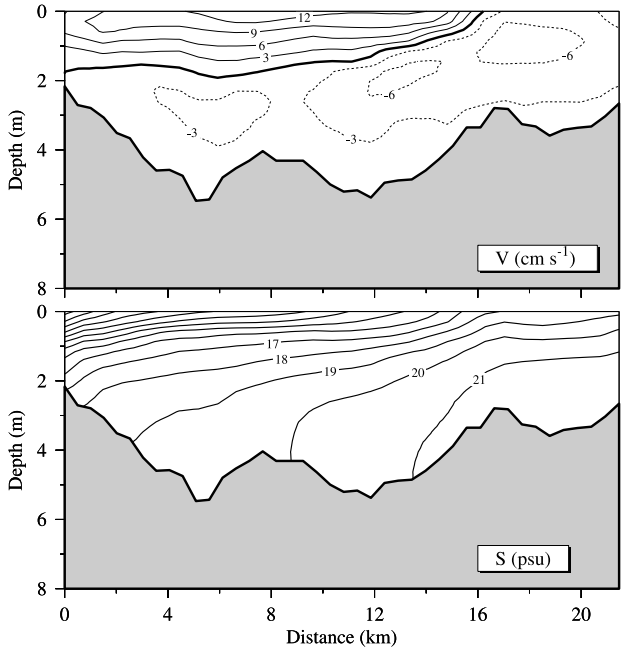

Figure 8. Along-axis (section I of Figure 2) tide-averaged (top) current and (bottom) salinity distributions for the case of tides, plus rivers. The contour intervals on currents and salinity are 3 cm s^{-1} and 1 psu, respectively.

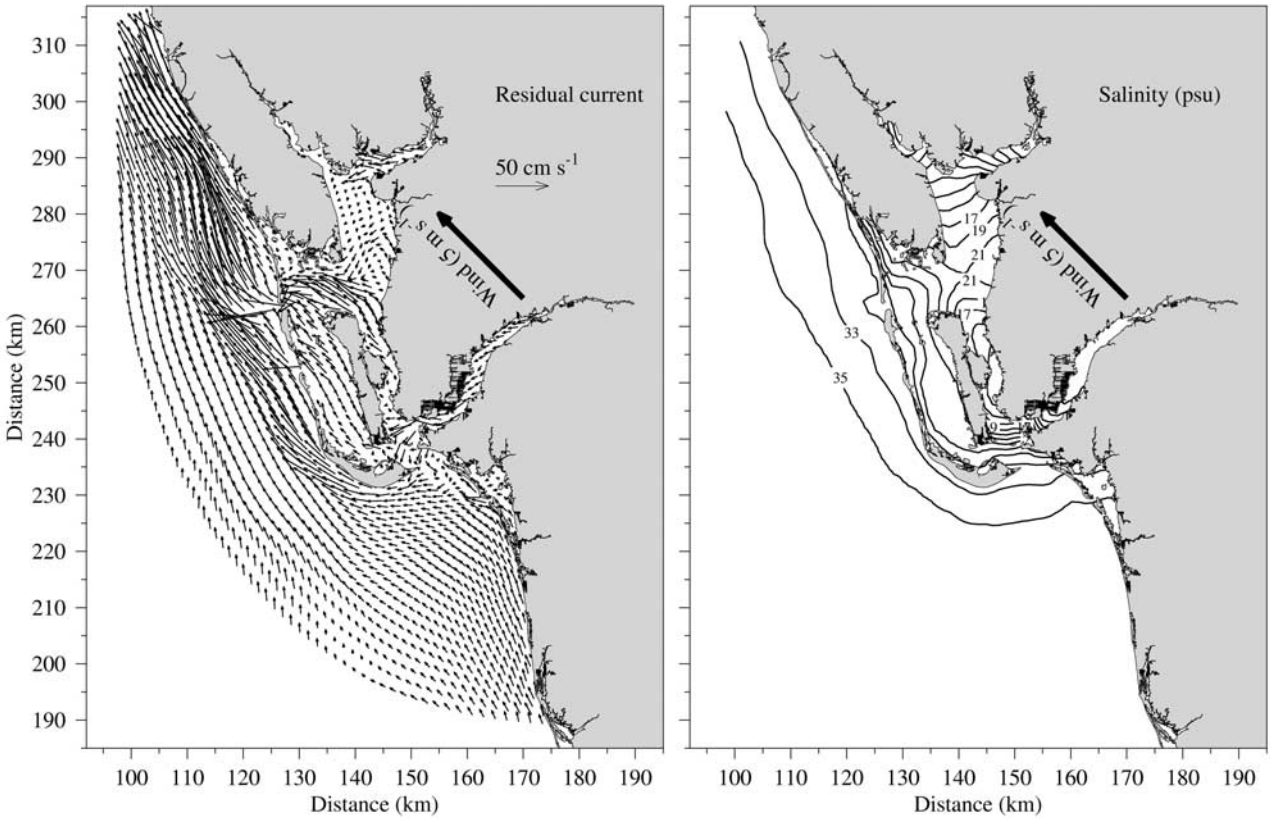

Figure 9. Tide-averaged surface (left) current vector and (right) salinity maps for the case of tides, plus rivers, plus a 5 m s^{-1} downwelling favorable wind. The contour interval for salinity is 1 psu, and the vectors are plotted at every third grid point.

[26] Tide-averaged surface current and salinity fields for downwelling favorable (and estuary circulation opposed) southeasterly winds are shown in Figure 9. Substantial differences from the no wind case are seen, both in the estuary and on the innershelf. In the estuary, surface currents that had been flowing in the direction opposite to the winds are reduced from Figure 7 and the salinities are higher throughout. Also seen is a communication of water from the SCB to the CH compartments of the estuary since the winds are able to overcome the constrictions of Matlacha Pass and Pine Island Sound. Thus, under downwelling favorable winds the SCB and CH sides are no longer independent systems. On the innershelf we see the salinity isolines are more closely packed along the coastline, and this concentrates the coastal jet within the region of offshore salinity gradient for three reasons. First, the steric effect of the offshore salinity gradient adds constructively with the wind-induced setup of the sea surface slope. Second, momentum is advected onshore concentrating the jet nearer to the coast. Third, by decreasing the near-bottom flow (through thermal wind shear) bottom friction is decreased, allowing for larger near surface currents.

[27] The vertical structure of the tide-averaged along-axis currents and salinity within the estuary are also modified (Figure 10). Relative to Figure 8 the net surface flow is now miniscule and the primary outlet for fresh water is at middepth, driven largely by the barotropic pressure head set up to balance the wind stress. The salinity isolines are

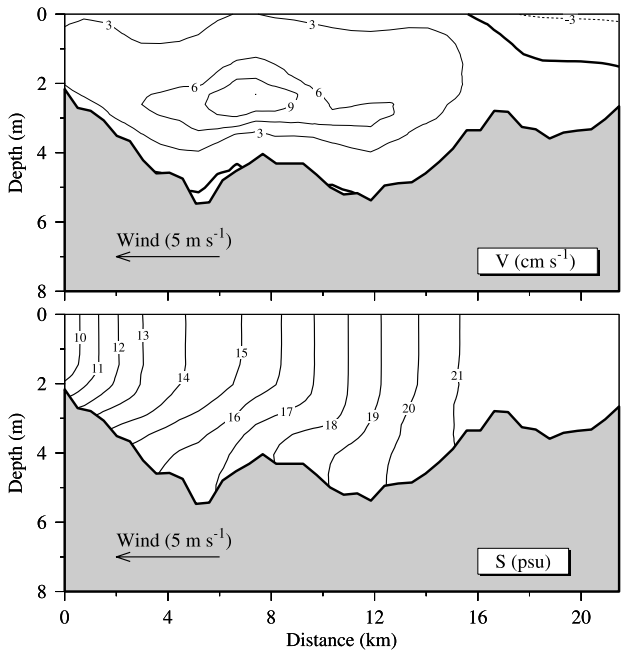

Figure 10. Along-axis (section I of Figure 2) tide-averaged (top) current and (bottom) salinity distributions for the case of tides, plus rivers, plus a 5 m s^{-1} downwelling favorable wind. The contour intervals on currents and salinity are 3 cm s^{-1} and 1 psu, respectively.

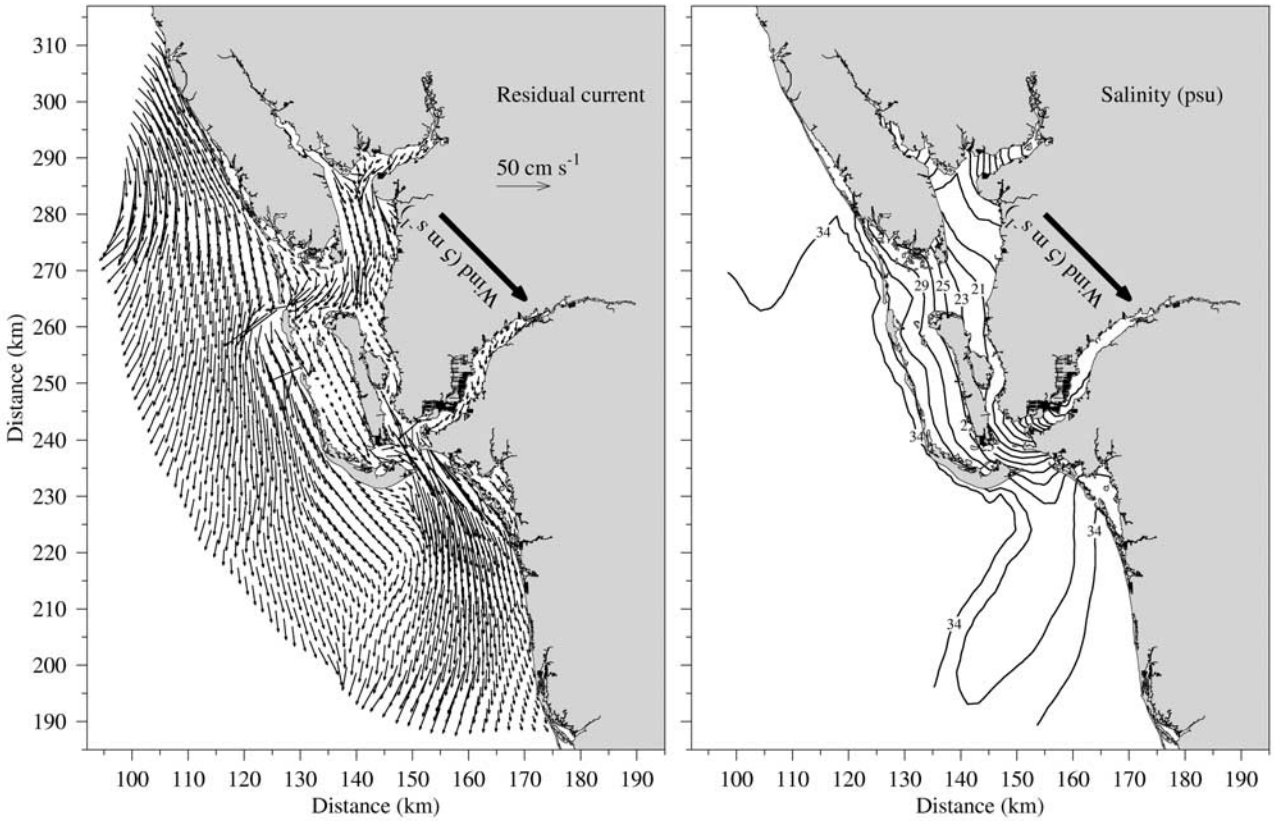

Figure 11. As in Figure 9 except a 5 m s^{-1} upwelling favorable wind.

now mostly vertical since wind stress induced mixing from the sea surface complements tide induced mixing from the bottom. Moreover, along with mixing by shear instability, mixing also occurs by convective overturning since the winds cause higher-salinity water from the lower reaches of the estuary to override lower-salinity water in the higher reaches of the estuary. By affecting both the pressure gradient distributions and the origins of mixing winds are highly effective at changing the estuarine circulation.

[28] Upwelling favorable (and in concert with the estuary circulation) winds also modify the circulation and salinity fields, but in very different ways (Figures 11 and 12). In the estuary the surface currents increase by the additive effects of winds and gravitational convection, and the salinity isolines are shifted southward. As is the case for downwelling favorable winds the two estuary compartments (CH and SCB) connect across Matlacha Pass and Pine Island Sound. Outside the estuary the along-shore current is broader than is the case of downwelling favorable winds. This is attributed to the lack of across-shore directed salinity gradient (except for south of the SCB mouth) together with an offshore advection of momentum that tends to broaden rather than concentrate the coastal jet. The fresh water efflux is now primarily out of SCB.

[29] The vertical structure of the tide-averaged along-axis currents and salinity (Figure 12) under upwelling favorable winds differs from either the no wind (Figure 8) or the downwelling favorable cases (Figure 10). With additive wind and gravitational convection the two-layered flow is increased and distributed more equally over the water column. Salinity isolines, rather than being nearly vertical, are now nearly horizontal by increased advection in the direction of the gravitation convection. A tendency for convective overturning also occurs in the upper reaches of

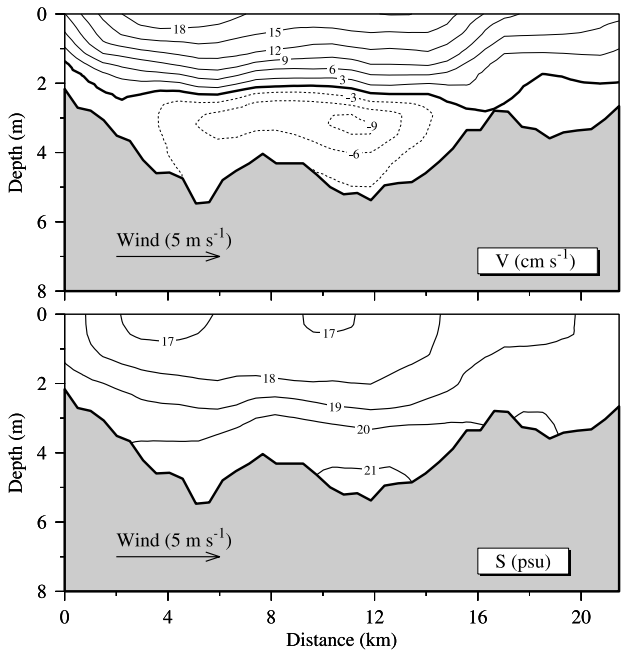

Figure 12. As in Figure 10 except a 5 m s^{-1} upwelling favorable wind.

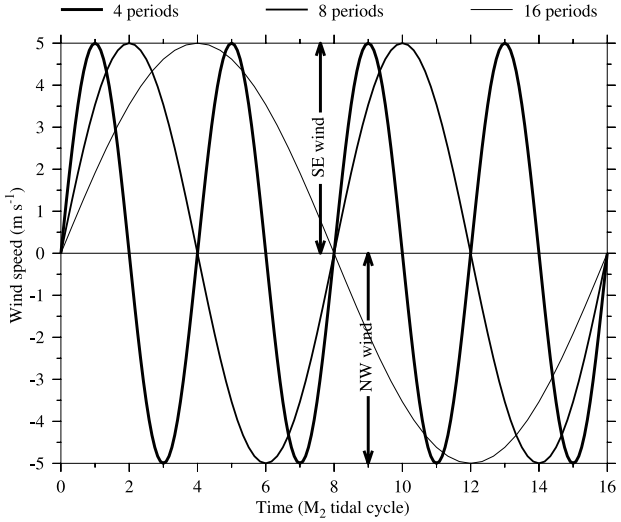

Figure 13. Wind variations used in the oscillatory wind experiments. Positive is downwelling favorable and negative is upwelling favorable.

the section as saltier water upwells and proceeds back toward the south tending to override fresher water.

[30] The increase in the two-layered flow, and consequently the increase in the horizontal advection of salinity, maintains the vertical stratification even in the presence of increased mixing by winds, although this stratification is weaker than that in the case without winds (Figure 8). With a vertical salinity gradient extending down to the bottom and stabilizing the water column there, the tidal mixing is also suppressed.

[31] In either case (southeasterly, downwelling favorable or northwesterly, upwelling favorable) we see that spatially uniform, steady winds largely alter the circulation and salinity structures of the CH estuary. Given these findings we next look at the effects of oscillatory winds typical of extratropical weather propagating through the region.

6. Tides, Plus Rivers, Plus Oscillatory Downwelling/Upwelling Winds

[32] As in section 5 we use a wind speed of 5 m s^{-1}, but instead of maintaining constant southeasterly or northwesterly winds we allow the winds to oscillate about a zero mean value with periodicities of 4, 8, and 16 M_2 cycles (Figure 13). These oscillatory winds are added after the model is spun up for tides over 10 M_2 cycles and for tides, plus rivers over another 120 M_2 cycles. The model is then run for 10 wind cycles (i.e., 40, 80, and 160 M_2 cycles for wind periods of 4, 8, and 16 M_2 cycles, respectively), after which the outputs are filtered to remove oscillations occurring on timescales shorter than 36 hours and then averaged over the full 10 wind cycles. We give results at the times of the maximum upwelling and downwelling wind phases and averaged over all cycles.

[33] At the maximum downwelling favorable phase of the wind cycle (Figure 14a), the near-surface speed decreases with increasing wind period. For example, the maximum upstream flow speed of about 0.24 m s^{-1} for the 4 M_2 cycle wind period, decreases to 0.12 m s^{-1} and 0.09 m s^{-1} for the 8 and 16 M_2 cycle wind periods, respectively. The salinity structure is also related to wind period, with the vertical stratification decreasing with increasing wind period. These results are consistent with the findings under constant winds. Downwelling favorable winds oppose the gravitational convection. For short-period oscillations the upstream current can accelerate with little opposition by an ensuing surface pressure gradient force. With increasing period the surface pressure gradient can set up to oppose the accelerating surface current, thereby reducing its magnitude. Similarly, increasing the wind period provides more time to transport higher-salinity water from the lower to the higher reaches of the estuary, which causes the salinity isolines to rotate more vertical.

[34] The vertical structure of the circulation and salinity for the maximum upwelling favorable winds are also a function of wind period (Figure 14b). The along-axis flow magnitude decreases with increasing period in part due to an opposing surface pressure gradient force, but also due to a decrease in the baroclinic portion of the pressure gradient force as the salinity isolines become more horizontal. The direct affects of the wind on both the barotropic (surface slope) and the baroclinic (isohaline slope) portions of the pressure gradient largely outweigh those by gravitational convection alone (the no wind case). In the CH, as in other estuaries, winds, even of modest magnitude, can dominate the tide-averaged flow and the resulting material property fields.

[35] Given that the tide-averaged, along-axis velocity and salinity fields are sensitive to the oscillatory wind period it is natural to ask whether or not the tide and oscillatory wind averaged net estuarine circulation and salinity fields are. As shown by Figure 14c, this sensitivity to the oscillatory wind period is much less perceptible. All three along-axis velocity and salinity panels look alike with a two-layered estuarine circulation and salinity stratification somewhat similar to the no wind case of Figure 8. Because of the added mixing by the winds over that by the tides and rivers alone the vertical salinity gradient is less, as is the magnitude of the gravitational convection. This begs the question of what determines the magnitude of the estuarine circulation under the combined effects of tides, rivers, and winds, each of which contribute to the averaged distributions of pressure gradient driving and frictional retarding forces. We treat this topic in a separate study on the energetics of the CH estuary [*Weisberg and Zheng*, 2003], which shows that the net estuarine circulation at first increases with increasing mixing and then decreases when the rate of energy input to turbulence production exceeds the rate of work against buoyancy.

[36] Oscillatory winds and tides also affect net material transports. We illustrate this by considering the up-estuary salt flux integrated across section II of Figure 2. Comparative results are given for the cases of tides and rivers and tides, rivers, and 5 m s^{-1} oscillatory winds (Figure 15 (top) and 15 (bottom), respectively). We first note that the instantaneous salt flux varies on all forcing function timescales. Here we calculate a nontidal up-estuary salt flux (using a 36 hour low-pass filter on the integrated product of the up-estuary velocity component and salinity), which we then further average over 80 M_2 cycles to get the mean and the horizontal Reynolds' contributions. We define the mean

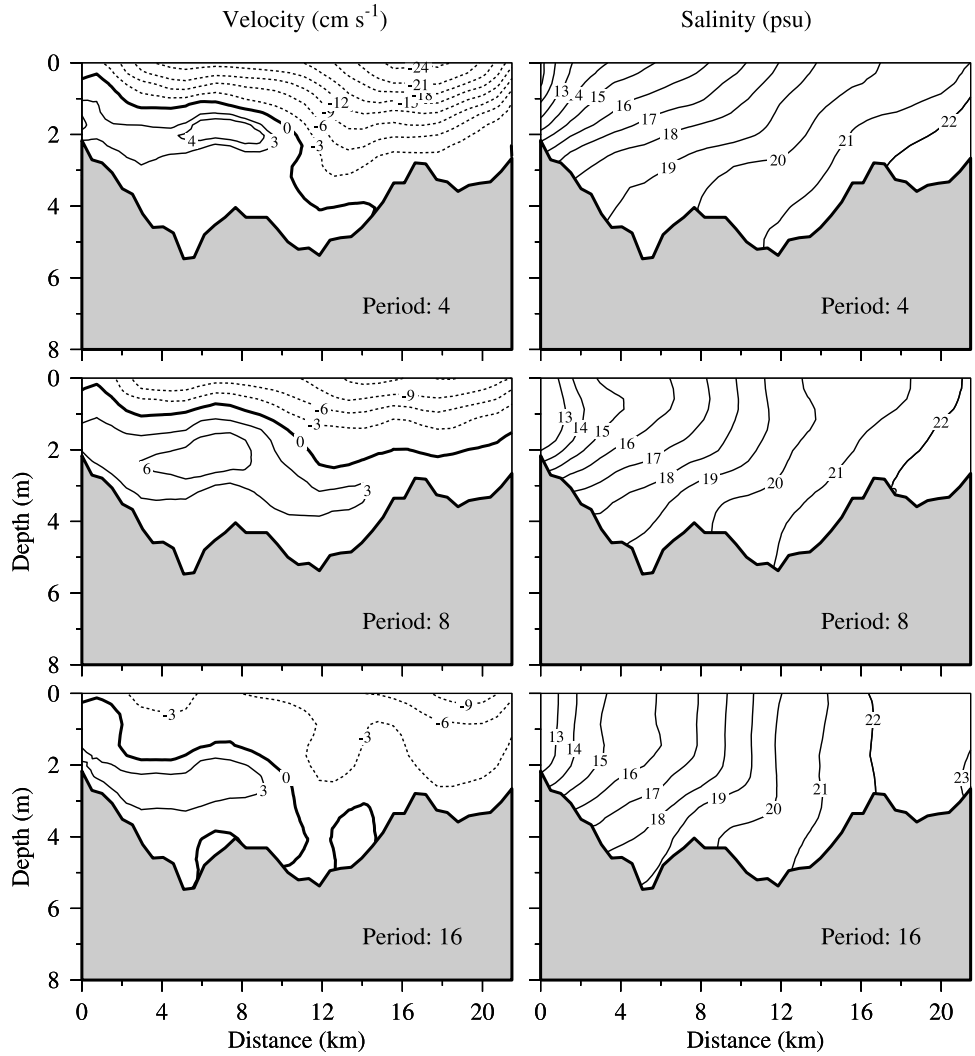

Figure 14a. Along-axis (section I of Figure 2) (left) current and (right) salinity distributions sampled (after filtering with a 36 hour low-pass filter) at the wind cycle phase corresponding to maximum downwelling favorable wind speed for the oscillatory wind periodicities of (top) 4, (middle) 8, and (bottom) 16 M_2 cycles. The contour intervals on currents and salinity are 3 cm s^{-1} and 1 psu, respectively.

contribution as the integrated product of the mean up-estuary velocity component and the mean salinity by gravitational convection, and we define the horizontal Reynolds' contribution as the integrated product of the deviations about these means. The record length mean of the nontidal salt flux is the sum of these two contributions.

[37] Without winds we find a spring to neap tide modulation in the nontidal salt flux, and upon averaging this we see that the record length mean salt flux is more than twice as large as the salt flux by the mean gravitational convection. The difference between these two is the Reynolds' flux, in this case due to tidal rectification [e.g., *Lewis and Lewis*, 1983; *Geyer and Nepf*, 1996]. With winds we find a nontidal salt flux modulation on the timescales of both the winds (in this case with an 8 M_2 cycle periodicity) and the spring to neap tide cycle, but only a slightly larger difference (the Reynolds' contribution) between the record length mean salt flux and the portion by gravitational convection. From these comparative findings we conclude that the Reynolds' salt flux is primarily a consequence of tidal rectification. While not shown, increasing the wind speed increases the Reynolds' contribution, but decreases the contribution by gravitational convection by a slightly larger amount such that the record length mean salt flux decreases. This arises because the mean circulation by gravitational convection [*Weisberg and Zheng*, 2003] and the correlation between the fluctuating velocity and salinity values are both sensitive to wind speed.

7. Summary and Conclusions

[38] The circulation of the CH estuary, driven by tides, rivers, and winds, is explored using a three-dimensional, primitive equation model. Tidal forcing is from the shelf through the inlets, and we consider the M_2, S_2, K_1, and O_1 constituents that account for some 95% of the WFS tidal variance. River discharges include the spring 1998 mean values for the Peace, Myakka, and Caloosahatchee Rivers.

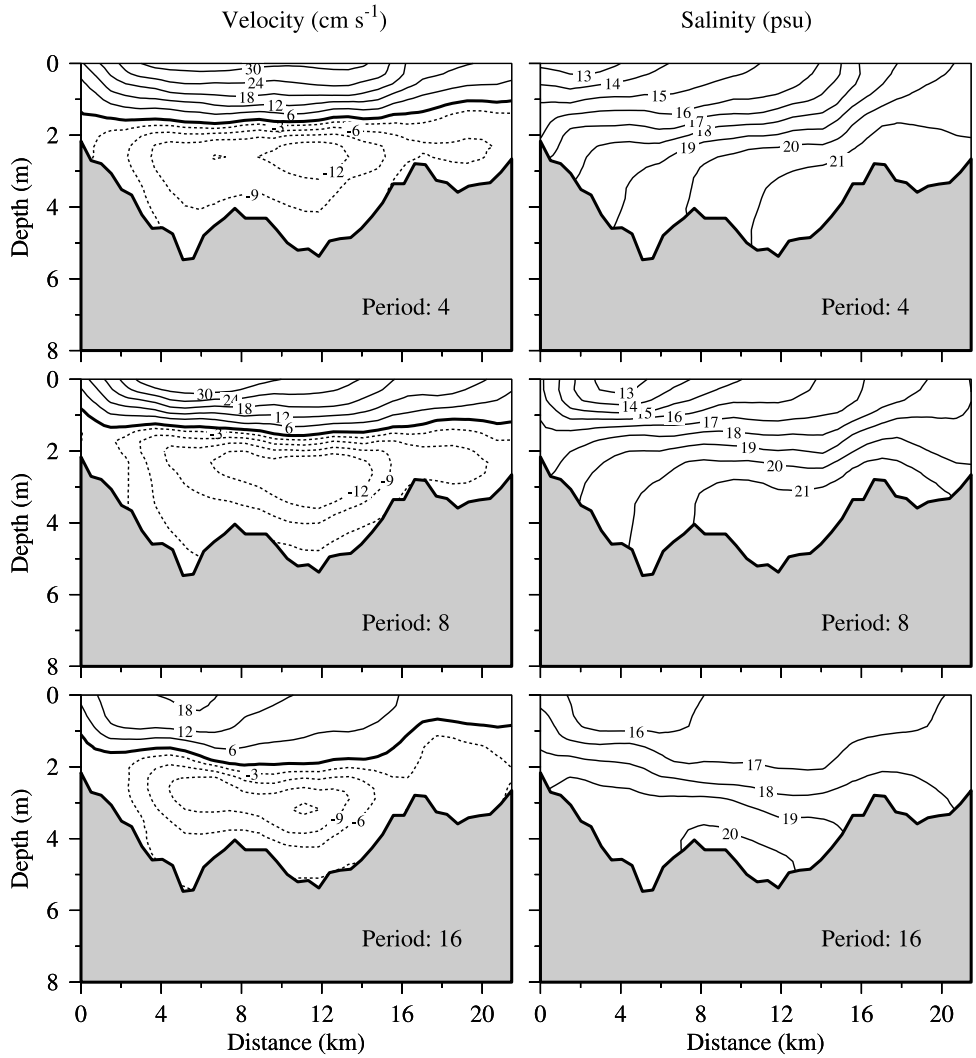

Figure 14b. As in Figure 14a except at maximum upwelling favorable wind speed.

Wind effects are considered for upwelling or downwelling favorable winds that are either held constant or allowed to oscillate with varying periodicities. Each of these factors is sequentially added to look at their individual and collective influences.

[39] Comparisons between the model and data at two tide gauges and one moored velocity station demonstrate the legitimacy of the open boundary forcing. We find that the tidal currents are impacted by the estuary's geometry, that the flows are asymmetrical and ebb dominant (during spring tides), and that the largest speeds occur across the BGP. Tidal amplitude and phase variations across the inlets and throughout the estuary system are by a combination of Bernoulli effect, wave propagation, and dissipation.

[40] River inflows, when coupled with tide-induced mixing, result in a nontidal estuarine circulation with a relatively fresh outflow atop a relatively salty inflow. The Coriolis acceleration causes the water on the western side of the CH portion of the estuary to be of lower salinity than on the eastern side. Similarly, the net outflow favors the western side while the net inflow favors the eastern side by a small amount. Under the influence of tides and rivers we find that the CH and the SCB portions of the estuary behave almost independently because of the shallowness of their connecting Matlacha Pass and Pine Island Sound.

[41] Winds affect the estuary in two ways. First, regardless of direction, winds increase the vertical mixing by imposing a stress at the surface. Second, winds provide an additional force that, depending on direction, may act either in concert with, or opposed to, the net pressure gradient force. Thus winds alter the CH estuary circulation driven by tides and rivers alone. For constant downwelling favorable winds (opposing the gravitational convection) the estuary becomes well mixed. For upwelling favorable winds (adding to the gravitational convection) stratification is maintained, but reduced from the no wind case because of increased mixing. The CH and SCB portions of the estuary also communicate for either wind directions. The instantaneous model results for oscillatory winds are sensitive to the oscillation period because of response times relative to the wind cycle. In contrast, the tide- and wind-averaged results are nearly independent of

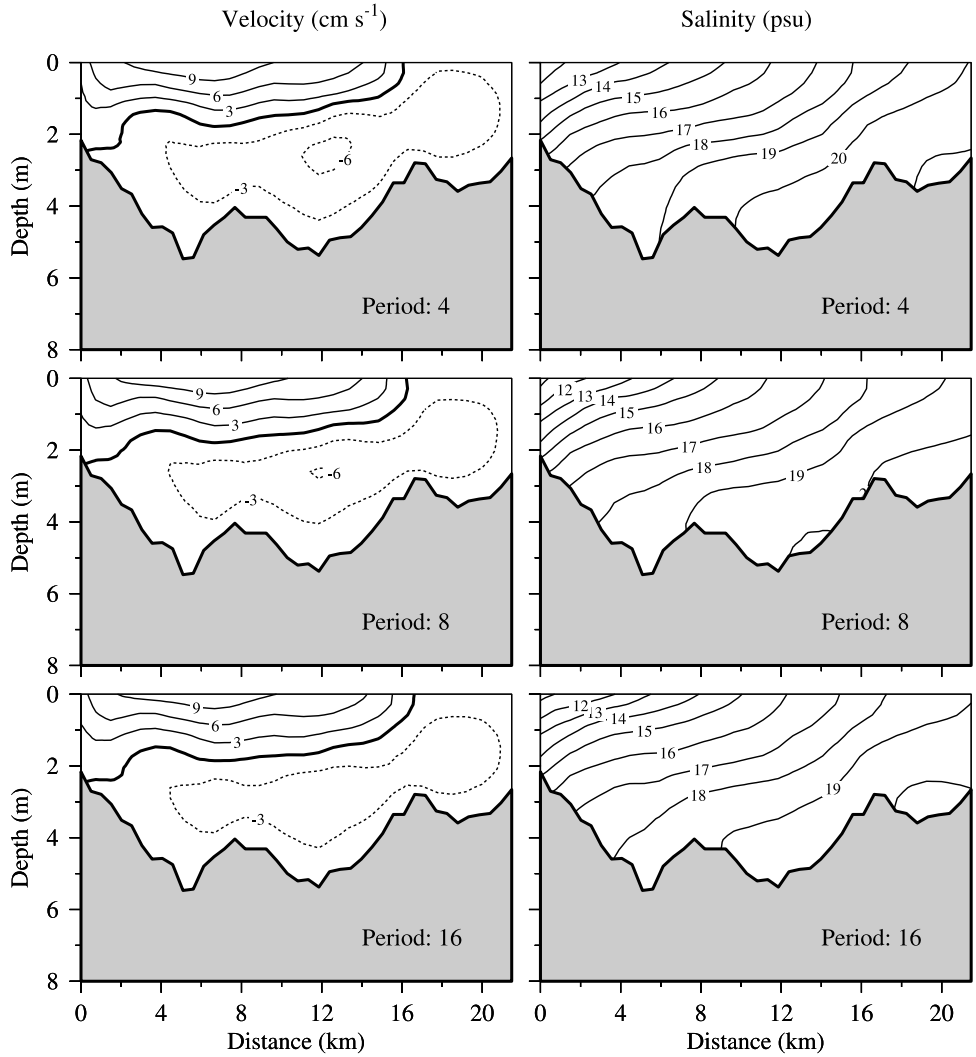

Figure 14c. Along-axis (section I of Figure 2) net tide- and wind-averaged (over 10 wind cycles) (left) current and (right) salinity distributions for the oscillatory wind periodicities of (top) 4, (middle) 8, and (bottom) 16 M_2 cycles. The contour intervals on currents and salinity are 3 cm s^{-1} and 1 psu, respectively.

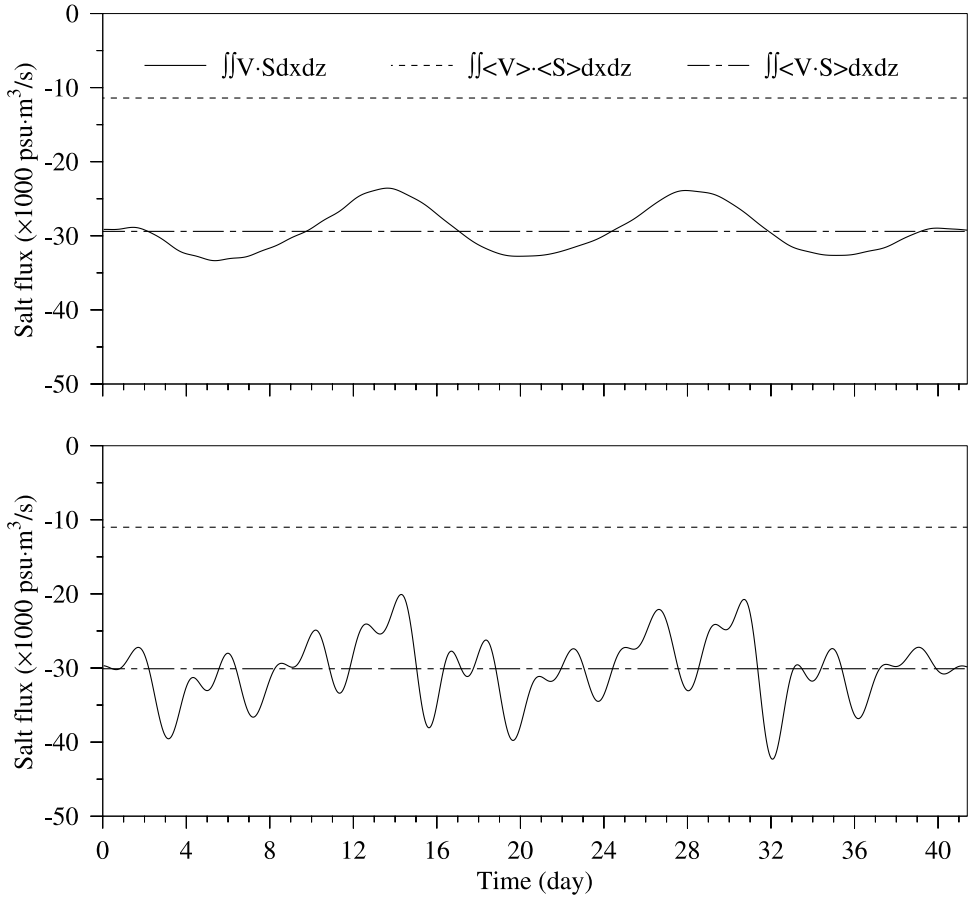

Figure 15. Up-estuary salt flux integrated across section II of Figure 2: (top) Tides and rivers only, and (bottom) tides, plus rivers, plus 5 m s^{-1} oscillatory winds. Three lines are shown for either case. The solid, time-varying lines are the low-pass-filtered (nontidal) salt flux that consists of contributions by the mean gravitational convection (the dashed lines) and the Reynolds' fluxes due to rectification by either the tides or by the tides plus winds (the difference between the dashed line and the dot-dashed line).

period. Here the dependence is on wind speed since that sets the level of turbulent mixing [*Weisberg and Zheng*, 2003].

[42] The net up-estuary salt flux consists of mean and Reynolds' contributions. With tides and rivers only the contribution by the Reynolds' salt flux due to tidal rectification is more than twice that of the mean gravitational convection. Oscillatory winds modify this salt flux partition (depending on wind speed), but the Reynolds fluxes remain primarily by tidal rectification. Similar arguments apply to transports of nutrients and other biologically important variables.

[43] In summary, the CH estuary circulation and salinity fields respond to a combination of tides, rivers, and winds. Since the circulation and salinity variances are large in time and space, both in the estuary and on the adjacent WFS, it follows that all other material properties (nutrients, plankton, fish larvae, etc.) will also have large variance in response to external forcing. Additional data are needed to test the findings herein and to support multidisciplinary ecosystems studies of the estuary.

[44] **Acknowledgments.** This research was supported by the Office of Naval Research under grants N00014-98-1-0158 and N00014-02-1-0972. The encouragement of E. Estevez, Mote Marine Laboratory, is appreciated.

References

Aubrey, D. G., and P. E. Speer (1985), A study of non-linear tidal propagation in shallow inlet/estuarine systems, part I: Observations, *Estuarine Coastal Shelf Sci.*, *21*, 185–205.

Blumberg, A. F. (1993), A primer of ECOM-si, technical report, 73 pp., HydroQual, Mahwah, N. J.

Blumberg, A. F., and G. L. Mellor (1987), A description of a three-dimensional coastal ocean circulation model, in *Three-Dimensional Coastal Ocean Models*, *Coastal Estuarine Sci.*, vol. 4, edited by N. Heaps, pp. 1–16, AGU, Washington, D. C.

Blumberg, A. F., and D. W. Pritchard (1997), Estimates of the transport through the East River, New York, *J. Geophys. Res.*, *102*, 5685–5703.

Blumberg, A. F., R. P. Signell, and H. L. Jenter (1993), Modeling transport processes in the coastal ocean, *J. Mar. Environ. Eng.*, *1*, 31–52.

Cameron, W. M., and D. W. Pritchard (1963), Estuaries, in *The Sea*, vol. 2, *The Composition of Seawater*, edited by M. N. Hill, pp. 306–324, John Wiley, Hoboken, N. J.

Casulli, V. (1990), Semi-implicit finite-difference methods for the two-dimensional shallow water equation, *J. Comput. Phys.*, *86*, 56–74.

Chen, C., and R. C. Beardsley (1995), A numerical study of stratified tidal rectification over finite-amplitude banks, I: Symmetric banks, *J. Phys. Oceanogr.*, *25*, 2090–2110.

Chen, C., and R. C. Beardsley (1998), Tidal mixing and cross-frontal particle exchange over a finite amplitude asymmetric bank: A model study with application to Georges Bank, *J. Mar. Res.*, *56*, 1163–1201.

Chen, C., L. Zheng, and J. Blanton (1999), Physical processes controlling the formation, evolution, and perturbation of the low-salinity front in the inner shelf off the southeastern United States: A modeling study, *J. Geophys. Res.*, *104*, 1259–1288.

Doering, P. H., and R. H. Chamberlain (1999), Water quality and source of freshwater discharge to the Caloosahatchee estuary, Florida, *J. Am. Water Resour. Assoc.*, *35*, 793–806.

Friedrichs, C. T., and O. S. Madsen (1992), Nonlinear diffusion of the tidal signal in frictionally dominated embayments, *J. Geophys. Res.*, *97*, 5637–5650.

Foreman, M. G. G. (1977), Manual for tidal heights analysis and prediction, *Pac. Mar. Sci. Rep. 77-10*, Inst. of Ocean Sci., Patricia Bay, Sidney, B. C., Canada.

Foreman, M. G. G. (1978), Manual for tidal current analysis and prediction, *Pac. Mar. Sci. Rep. 78-6*, Inst. of Ocean Sci., Patricia Bay, Sidney, B. C., Canada.

Geyer, W. R., and H. Nepf (1996), Tidal pumping of salt in a moderately stratified estuary, in *Buoyancy Effects on Coastal and Estuarine Dynamics*, *Coastal Estuarine Stud.*, vol. 53, edited by D. G. Aubrey and C. T. Friedrichs, pp. 213–226, AGU, Washington, D. C.

Goodwin, C. R. (1996), Simulation of tidal-flow, circulation, and flushing of the Charlotte Harbor estuarine system, Florida, *U. S. Geol. Surv. Water Resour. Invest. Rep., 93-4153*, 92 pp.

Goodwin, C. R., and D. M. Michaelis (1976), Tides in Tampa Bay, Florida: June 1971 to December 1973, *U. S. Geol. Surv. Open-File Rep., FL-75004*, 338 pp.

He, R., and R. Weisberg (2002), Tides on the west Florida shelf, *J. Phys. Oceanogr.*, *32*, 3455–3473.

Hellerman, S., and M. Rosenstein (1983), Normal monthly wind stress over the world ocean with error-estimates, *J. Phys. Oceanogr.*, *13*, 1093–1104.

Lewis, R. E., and J. O. Lewis (1983), The principal factors contributing to the flux of salt in a narraw, partially stratified estuary, *Estuarine Coastal Shelf Sci.*, *16*, 599–626.

Li, Z., and R. H. Weisberg (1999), West Florida continental shelf response to upwelling favorable wind forcing: 2. Dynamics, *J. Geophys. Res.*, *104*, 23,427–23,442.

Mellor, G. L., and T. Ezer (1991), A Gulf Stream model and an altimetry assimilation scheme, *J. Geophys. Res.*, *96*, 8779–8795.

Mellor, G. L., and T. Yamada (1982), Development of a turbulence closure model for geophysical fluid problems, *Rev. Geophys.*, *20*, 851–875.

Smolarkiewicz, P. K. (1984), A fully multidimensional positive definite advection transport algorithm with small implicit diffusion, *J. Comput. Phys.*, *54*, 325–362.

Wang, D. P. (1979), Wind-driven circulation in the Chesapeake Bay, winter 1975, *J. Phys. Oceanogr.*, *9*, 564–572.

Weisberg, R. H. (1976), The nontidal flow in the Providence River of Narragansett Bay: A stochastic approach to estuarine circulation, *J. Phys. Oceanogr.*, *6*, 721–734.

Weisberg, R. H., and W. Sturges (1976), Velocity observations in the west passage of Narragansett Bay: A partially mixed estuary, *J. Phys. Oceanogr.*, *6*, 345–354.

Weisberg, R. H., and L. Zheng (2003), How estuaries work: A Charlotte Harbor example, *J. Mar. Res.*, *61*, 635–657.

Zheng, L., C. Chen, and H. Liu (2003), A modeling study of the Satilla River estuary, Georgia, part I: Flooding/drying process and water exchanges over the salt marsh-estuary-shelf complex, *Estuaries*, *26*, 651–669.

R. H. Weisberg and L. Zheng, College of Marine Science, University of South Florida, 140 Seventh Avenue South, St. Petersburg, FL 33701, USA. (weisberg@marine.usf.edu)